arXiv:1407.6862v1 [quant-ph] 25 Jul 2014

Dynamics of an open quantum system interacting with a quantum environment

Athreya Shankar, S Lakshmibala and V Balakrishnan

Department of Physics, Indian Institute of Technology Madras, Chennai 600 036, India

Abstract. We examine the dynamics of subsystems of bipartite and tripartite quantum systems with nonlinear Hamiltonians. We consider two models which capture the generic features of open quantum systems: a three-level atom interacting with a single-mode radiation field, and a three-level atom interacting with two field modes which do not directly interact with each other. The entanglement of specific initially unentangled states of the atom-field system is examined through the time-varying subsystem von Neumann entropy (SVNE). The counterparts of near-revivals and fractional revivals of the initial state are clearly identifiable in the SVNE in all cases where revival phenomena occur. The Mandel Q parameter corresponding to the photon number of a radiation field is obtained as a function of time in both models. In those cases where revivals are absent, a time series analysis of the mean photon number reveals a variety of ergodicity properties (as manifested in return maps, recurrence-time distributions and Lyapunov exponents), depending on the strength of the nonlinearity and the degree of coherence of the initial state of the radiation field(s).

PACS numbers: 42.50.-p, 03.67.-a, 03.67Mn, 42.50Dv, 05.45.-a, 05.45.Tp

1. Introduction

Quantum systems governed by nonlinear Hamiltonians can display a wide variety of nonclassical effects such as revivals and fractional revivals during their temporal evolution [1]. The dynamics of subsystems of quantum systems depends strongly on the nature of their interactions with the quantum 'environment' to which they are exposed. The crucial point is the following. The full system remains in a pure state whose unitary time development is governed by an appropriate hermitian Hamiltonian. A subsystem, however, is described, in general, by a reduced density matrix that evolves through a dynamical map. This, in turn, could result in lossy interaction of the subsystem with the environment, leading to decoherence effects. The subsystem can effectively be modelled as a dissipative system.

A convenient framework to examine the rich dynamics of an open quantum subsystem is provided by specific bipartite and multipartite models of atom-field interactions. As we shall see, the dynamics of the field in such models differs considerably from that of an initial single-mode coherent state (CS) of the radiation field propagating in a nonlinear (Kerr) medium with an effective Hamiltonian [2, 3]

$$H_{\rm Kerr} = \hbar\chi {a^\dagger}^2 a^2. \tag{1}$$

Here, a and $a^\dagger$ are the usual photon annihilation and creation operators, and χ is a positive constant that sets a time scale. Exact revivals of the field state occur in this case at instants of time that are integer multiples of π/χ: at these instants an initial state returns to itself apart from an overall phase. Hence all expectation values also return to their initial values. Under specific conditions, fractional revivals could occur between two successive revivals: at these instants, the wave packet splits into a number of spatially distributed subpackets each of which closely resembles the initial wave packet. Revivals have been understood in a general setting [4] for an arbitrary initial superposition of photon number states, and revival phenomena have been discussed in a wide class of systems [1–3], [5–8]. In most of these earlier studies the initial state is a CS $|\alpha\rangle$, where $a|\alpha\rangle = \alpha|\alpha\rangle$ and $\alpha \in \mathcal{C}$.

It has further been established [9,10] that in the case of the Kerr Hamiltonian in (1), signatures of the occurrence of revivals and fractional revivals of the radiation field are manifested in the mean and higher moments of appropriate observables. The field states considered in this case are CS as well as photon-added coherent states (PACS). The m-photon-added coherent state (m-PACS) $|\alpha, m\rangle$ is obtained by an m-fold application of the photon creation operator on the CS $|\alpha\rangle$, and normalizing the resultant state [6]. The PACS family displays precisely quantifiable departure from coherence, and hence lends itself to a systematic examination of the role of coherence in wave packet dynamics. Experimental identification and characterization of the single photon-added coherent state [11] using quantum state tomography has added more impetus to such studies.

In contrast to this, even in the simplest bipartite atom-field system modelled by a nonlinear Hamiltonian involving both field and atom operators explicitly, exact revivals of the initial state need not occur. The dynamics in this case is enriched by the

phenomenon of quantum entanglement. Even if the initial state of the system is an unentangled direct product of the field and atom states, entanglement occurs during temporal evolution, and exact revivals of the initial state are generically absent. Wave packet revivals would be even less probable in a multipartite system, in general.

The occurrence of near-revivals therefore is the best that one can hope for in general in these cases. In bipartite models of atom-field interactions, the appearance of such near-revivals would be crucially dependent on the ratio of the strength of the nonlinearity to the strength of the interaction between the two subsystems. A model Hamiltonian describing a multi-level nonlinear atomic medium interacting with a single-mode radiation field [12] has been examined earlier [13], illustrating when near-revivals occur in bipartite systems, and how the subsystem von Neumann entropy (SVNE) and the system linear entropy (SLE) mirror the appearance of revivals and fractional revivals. These results indicate that, for an initial coherent state of the field, if the strength of the nonlinearity is significantly smaller than the strength of atom-field interaction, both the SVNE and SLE show pronounced dips at the near-revival time period T_{rev}, and fractions 1/2, 1/3, 1/4 and 2/3 of T_{rev} when fractional revivals occur. In contrast, for the same numerical values of the nonlinearity and coupling strengths, if the initial state of the radiation field is a PACS, the SVNE at any instant also increases in comparison with the case of an initial CS, and even near-revivals disappear.

The latter situation raises interesting questions pertaining to the dynamical behaviour of the expectation values of observables. For instance, an experimentally relevant quantity such as the mean photon number of a radiation field [14] could move far away from its initial value over a sufficiently long period of time, in a situation where even near-revivals are absent. A time series analysis of the mean photon number would reveal a diversity of ergodicity properties of the observable. Such an investigation has been carried out [15] in the framework of the bipartite model considered in [12]. It is found that, if the strength of the nonlinearity is significantly more than the interaction strength, then, depending on the level of departure from coherence of the initial state, the mean photon number could even display exponential instability indicated by a positive Lyapunov exponent obtained through the time series analysis.

Extensive work has been carried out to understand the ergodicity properties of classical dynamical systems, by examining return-time statistics of dynamical variables to coarse-grained cells in phase space, and rigorous results established on Poincaré recurrences [16]. Important and interesting results are known on the recurrence properties of classical systems such as Hamiltonian systems, measure-preserving maps, and dissipative maps. In conservative classical systems it has been established that universal asymptotic properties including power-law recurrence-time distributions arise due to the non-uniform nature of invariant sets in phase space and 'stickiness' of remnants of invariant tori [17]. Again, detailed studies of recurrence-time distributions in low-dimensional maps enable us to differentiate clearly between varying degrees of randomness ranging from quasiperiodicity through intermittent behavior to fully-developed chaos [18,19]. Apart from these, recurrence plots [20] are used to analyze the

dynamical behaviour of classical variables.

Similar in-depth investigations on the behaviour of quantum observables are scant. As is the case in classical systems, we would expect recurrence time statistics of quantum observables to complement information obtained through Lyapunov exponents deduced from a time series analysis of the observables. To carry out such studies, it is appropriate to consider the recurrence time distributions of the expectation values of suitable observables (such as the mean photon number) in models of atom-field interactions, to cells in a 'phase space' of these expectation values. An inherently quantum mechanical feature that arises in this approach is that the phase space is now effectively infinite-dimensional, as it involves the expectation values of all the relevant observables, their higher moments, and all correlators. In principle, the collective dynamics of all these variables needs to be analyzed. In practice, therefore, it is crucial to identify an adequately tractable and experimentally relevant observable (or a minimal set of such observables) whose dynamical properties may be investigated. When a quantum mechanical system is partitioned into subsystems, each subsystem can interact with the others (which constitute a quantum mechanical 'environment') in a complicated manner. The dynamics of observables will depend quite strongly on the specific initial state. The ergodicity properties of these observables can be quite complex. Such an approach facilitates the understanding of the ergodic behaviour of classical and quantum systems in a unified manner, and enables us to relate known results on Poincaré recurrences obtained from classical ergodic theory, on the one hand, and the temporal behaviour of quantum expectation values treated as 'classical' dynamical variables, on the other.

The results of such an investigation on the nonlinear bipartite model [12] of a multi-level atom (modelled by a nonlinear oscillator) interacting with a single-mode field in an initial CS or a PACS indicate [15, 21] that the first-return-time distribution is spiky for merely quasiperiodic dynamics, and exponential for long-term chaotic behaviour of the mean photon number. In this bipartite model, the Hilbert spaces of both the radiation field and the atom are essentially infinite-dimensional. The behaviour of the SVNE and a time series analysis of the mean photon number may be expected to be significantly different from the foregoing in the case of a more realistic three-level atom (implying an associated finite-dimensional Hilbert space) interacting with a radiation field. À priori we would expect that, for essentially the same ratio of the strength of the nonlinearity to that of the interaction, marked differences in the dynamics of the mean photon number would occur, as compared to those reported in [15].

Going further, we may generalize this bipartite system to one in which a three-level Λ- or V-type atom interacts with two radiation fields which do not directly interact with each other. Naturally, this tripartite system may be expected to display far richer dynamics than the bipartite models. While both the field modes have associated Hilbert spaces which are infinite-dimensional, the interaction proceeds through the very small number of channels supplied by the atom. This 'bottleneck' may also be expected to affect the dynamics strongly. We are also motivated by the fact that photon-counting

experiments on systems comprising a single atom interacting with laser light have already been realised (see, for instance, [22].

In this paper, we examine the dynamics of the field mode in two models describing the interaction between light and a three-level V-type atom. The first is a bipartite model of a single-mode radiation field interacting with the atom so as to enable transitions from either of the excited levels to the ground state of the atom. The second is a tripartite extension of this model, where two independent single-mode fields interact with the V-type atom. Denoting the excited states of the atom by $|1\rangle$ and $|2\rangle$, and the ground state by $|3\rangle$, one of the radiation modes induces $|1\rangle \leftrightarrow |3\rangle$ transitions, and the other induces $|2\rangle \leftrightarrow |3\rangle$ transitions. The ratio of the strength of the nonlinearity to the strength of the atom-field interaction is a controlling parameter. In both models the Hamiltonian is nonlinear in the field operators. The initial states of the field(s) that we consider are CS and PACS.

In Section 2, we examine the SVNE as a function of time for initially unentangled atom-field states, and obtain results on the subsequent entanglement dynamics as well as near-revival phenomena. We also find the time variation of the Mandel Q parameter (a measure of the deviation of the photon number from Poisson statistics). Wherever applicable, a comparison is made with corresponding results reported in [15] on the dynamics of a multi-level atom interacting with a single-mode radiation field.

In Section 3, we investigate the ergodicity properties of the mean photon number of the field in both these models for several different initial states. These show diverse kinds of behaviour, ranging from regular to chaotic, in the dynamics of the mean photon number of either field in the tripartite system. For our purposes, we have examined the mean photon number of the mode that induces $|1\rangle \leftrightarrow |3\rangle$ transitions in the atom.

In all the cases we consider, the strength of the nonlinearity has been set equal to a value which is significantly higher than the corresponding atom-field coupling strength. As in the case of [15], it turns out that such a parameter ratio regime ensures non-trivial dynamical behaviour of the mean photon number such as exponential instability, near-revivals, and so on. We conclude with a summary of the results and comment on possible experimental verification of some of the salient features deduced.

2. Entanglement dynamics in the bipartite and tripartite models

We begin with the bipartite model describing the interaction of a single-mode radiation field with a three-level V-type atom. Transitions occur between the two excited states and the ground state. Subsequently, we extend the model to a tripartite Hamiltonian where two different field modes couple to the two different excited states and induce transitions between these and the ground state. In both cases the field operators exhibit Kerr-type nonlinearity. Both the models that we consider are simplified versions of models which incorporate intensity-dependent couplings and non-zero detuning. For our present purposes, however, it suffices to take the interaction strength to be independent of the intensity of the field and set the detuning parameter

to zero. The three-level V-type atom consists of a ground state, labelled $|3\rangle$, and two excited states $|1\rangle$ and $|2\rangle$. Only $|3\rangle \leftrightarrow |1\rangle$, and the $|3\rangle \leftrightarrow |2\rangle$ transitions are allowed. Direct $|1\rangle \leftrightarrow |2\rangle$ transitions between the excited states are forbidden.

2.1. Interaction with a single field mode

The general Hamiltonian for the bipartite system which includes an intensity-dependent coupling and non-zero detuning is given (see, e.g., [23]) by

$$H = \sum_{j=1}^{3} \omega_j \sigma_{jj} + \Omega a^\dagger a + \chi a^{\dagger 2} a^2 + \lambda_1 (R\sigma_{13} + R^\dagger \sigma_{31}) + \lambda_2 (R\sigma_{23} + R^\dagger \sigma_{32}). \tag{2}$$

Here, $\sigma_{jj} = |j\rangle\langle j|$ where $|j\rangle$ is an atomic state, $\{omega_j\}$ are positive constants, Ω is the frequency of the field mode, χ is the anharmonicity parameter, and λ_1 and λ_2 are the field-atom coupling strengths controlling $|3\rangle \leftrightarrow |1\rangle$ and $|3\rangle \leftrightarrow |2\rangle$ transitions, respectively. $a^\dagger$ and a are the photon creation and annihilation operators, $N = a^\dagger a$, and $R = af(N)$, where $f(N)$ is a real-valued function that characterizes the intensity-dependent coupling. We set $\hbar = 1$ throughout. The Hamiltonian H in (2) is split into two mutually commuting parts according to $H = H_0 + H_1$, where

$$H_0 = \omega_3 I + \Omega N^{\rm tot}, \tag{3a}$$

$$H_1 = \chi a^{\dagger 2} a^2 - \Delta_1 \sigma_{11} - \Delta_2 \sigma_{22} + \lambda_1 (R\sigma_{13} + R^\dagger \sigma_{31}) + \lambda_2 (R\sigma_{23} + R^\dagger \sigma_{32}). \tag{3b}$$

Here $I = \sum_{j=1}^{3} \sigma_{jj}$ and $N^{\rm tot} = a^\dagger a + |1\rangle\langle 1| + |2\rangle\langle 2|$ (in a sense, the 'total number operator'). Δ_1 and Δ_2 are detuning parameters given by

$$\Delta_1 = \omega_3 - \omega_1 + \Omega \tag{4a}$$

$$\Delta_2 = \omega_3 - \omega_2 + \Omega. \tag{4b}$$

As already mentioned, we set the detuning parameters equal to zero, and assume that the coupling of the field to the atom is a constant independent of the intensity of the field, (i.e., $R = a$). For the sake of clarity, we outline below the salient steps in obtaining the state of the system at a subsequent time, given the initial state.

The eigenstates of H_0 are chosen as a basis, while H_1 is treated as an interaction Hamiltonian. Throughout this work, we take the initial state of the atom to be $|1\rangle$, and that of the field to be some specified superposition $\sum_{n=0}^{\infty} q_n |n\rangle$ of n-photon (Fock) states. We denote by $|j; n\rangle$ the direct product state in which the atom is in state $|j\rangle$ $(j = 1, 2, 3)$ and the field is in an n-photon state. Then (retaining the general notation of [23]), the state of the system in the interaction picture at any time $t \geq 0$ is of the form

$$|\psi(t)\rangle_{\rm int} = \sum_{n=0}^{\infty} q_n \Big\{ A_n(t) |1; n\rangle + B_n(t) |2; n\rangle + C_{n+1}(t) |3; n+1\rangle \Big\}. \tag{5}$$

The time-dependent coefficients $A_n(t)$, $B_n(t)$ and $C_{n+1}(t)$ satisfy the coupled differential equations

$$i\dot{A}_n = V_1 A_n + f_1 C_{n+1} \tag{6a}$$

$$i\dot{B}_n = V_1 B_n + f_2 C_{n+1} \tag{6b}$$

$$i\dot{C}_{n+1} = V_2 C_{n+1} + f_1 A_n + f_2 B_n, \tag{6c}$$

where

$$V_1 = \chi n(n-1), \quad V_2 = \chi n(n+1) \tag{7a}$$

$$f_1 = \lambda_1\sqrt{n+1}, \quad f_2 = \lambda_2\sqrt{n+1}. \tag{7b}$$

The trial solution $B_n \sim e^{i\mu t}$ gives us the following cubic equation for the characteristic frequency μ:

$$\mu^3 + x_1\mu^2 + x_2\mu + x_3 = 0, \tag{8}$$

where

$$x_1 = 2V_1 + V_2 \tag{9a}$$

$$x_2 = V_1(2V_2 + V_1) - f_1^2 - f_2^2 \tag{9b}$$

$$x_3 = -V_1(V_2V_1 - f_1^2 - f_2^2). \tag{9c}$$

This equation has three real roots given by

$$\mu_j = -\frac{x_1}{3} + \frac{2}{3}\sqrt{(x_1^2 - 3x_2)}\,\cos\left\{\theta + \frac{2}{3}(j-1)\pi\right\}, \quad (j = 1, 2, 3) \tag{10}$$

where

$$\theta = \frac{1}{3}\cos^{-1}\left\{\frac{9x_1x_2 - 2x_1^3 - 27x_3}{2(x_1^2 - 3x_2)^{\frac{3}{2}}}\right\}. \tag{11}$$

Substituting $B_n(t) = \sum_{j=1}^{3} b_j e^{i\mu_j t}$ in (6a)–(6c) gives

$$A_n(t) = \sum_{j=1}^{3} \frac{b_j}{f_2 f_1}\left\{(\mu_j + V_1)(\mu_j + V_2) - f_2^2\right\} e^{i\mu_j t}, \tag{12a}$$

$$C_{n+1}(t) = -\sum_{j=1}^{3} \frac{b_j}{f_2}(\mu_j + V_1)e^{i\mu_j t}. \tag{12b}$$

The coefficients b_j are given by

$$b_j = \frac{f_1 f_2}{(\mu_j - \mu_k)(\mu_j - \mu_l)}, \tag{13}$$

where, for each j, the indices k and l take the other two distinct values.

We now have the complete state of the system at time t. The density matrix $\rho(t)$ for the system can now be contructed, and the reduced density matrices $\rho_A(t)$ and $\rho_F(t)$ for the atom and field respectively can be obtained. These are given by

$$\langle 1|\,\rho_A(t)\,|1\rangle = \sum_{n=0}^{\infty} q_n q_n^* A_n A_n^* \tag{14a}$$

$$\langle 2|\,\rho_A(t)\,|2\rangle = \sum_{n=0}^{\infty} q_n q_n^* B_n B_n^* \tag{14b}$$

$$\langle 3|\,\rho_A(t)\,|3\rangle = \sum_{n=1}^{\infty} q_{n-1} q_{n-1}^* C_n C_n^* \tag{14c}$$

$$\langle 1|\,\rho_A(t)\,|2\rangle = \sum_{n=0}^{\infty} q_n q_n^* A_n B_n^* \tag{14d}$$

$$\langle 1|\,\rho_A(t)\,|3\rangle = \sum_{n=1}^{\infty} q_n q_{n-1}^* A_n C_n^* \tag{14e}$$

$$\langle 2|\,\rho_A(t)\,|3\rangle = \sum_{n=1}^{\infty} q_n q_{n-1}^* B_n C_n^*, \tag{14f}$$

and

$$\begin{aligned}\langle n|\,\rho_F(t)\,|n'\rangle &= q_n q_{n'}^* (A_n A_{n'}^* + B_n B_{n'}^*) \\ &\quad + (1-\delta_{n,0})(1-\delta_{n',0}) q_{n-1} q_{n'-1}^* C_n C_{n'}^*.\end{aligned} \tag{15}$$

Using these results, we now proceed to investigate numerically the temporal behaviour of the SVNE when the initial state of the radiation field is either a CS or a PACS. We have also computed the Mandel Q parameter as a function of time, for these initial states. For simplicity, we have set $\lambda_1 = \lambda_2 = \lambda$ (so that $f_1 = f_2$) in the numerics. As already stated, we work in a parameter regime where the nonlinearity in the field dominates over the atom-field interaction, by taking the ratio χ/λ to be 5. Consistent with the notation $|j; n\rangle$, we denote by $|1; \alpha\rangle$ a state in which the atom is in state $|1\rangle$ and the field is in a CS $|\alpha\rangle$. Similarly, $|1; \alpha, m\rangle$ $(m = 1, 2, \ldots)$ denotes a state in which the field is in an m-photon added PACS.

In figures 1(a)–(c) we have plotted the SVNE corresponding to the field subsystem, $-\mathrm{Tr}\ (\rho_F \log_2 \rho_F)$, as a function of the scaled time λt, for different initial states of the field. Note the different time scales in figure 1(a) and in figures 1(b), (c). It is seen from figure 1(a) that an initially unentangled state $|1; \alpha\rangle$ (with SVNE equal to zero) gets entangled over a very short time. Although this initial state does not revive fully at any later time, the SVNE drops to relatively small values almost periodically (when $\lambda t \approx 400, 800, \ldots$). In between these times marked oscillatory behaviour is seen in the SVNE with less-pronounced dips close to instants of approximate fractional revivals. Thus, signatures of near-revival phenomena are captured in the SVNE in this system,

even for the case of strong nonlinearity. This is to be contrasted with earlier results [13] on the system in [12] where, regardless of the initial state, plausible signatures of near-revival phenomena are seen in the SVNE only in the weak nonlinearity regime. The finite-dimensional Hilbert space of the V-type atom in the present model plays a crucial role in this regard. As in the cases reported in [13], any significant departure of the initial field state from coherence, or an initial CS with large $|\alpha|^2$, essentially erases even near-revivals. This is seen in figures 1(b) and (c): the SVNE never gets close to its initial value of zero at a later time.

Next, we turn to the Mandel Q parameter, defined as

$$Q = \frac{\langle (a^\dagger a)^2 \rangle - \langle a^\dagger a \rangle^2}{\langle a^\dagger a \rangle} - 1 \tag{16}$$

Q is a measure of the deviation of the photon number distribution from Poisson statistics (which is, of course, a hallmark of a CS). Figures 2(a)–(c) show Q as a function of time, for the same initial states and parameter values as above. Once again, the time scale in each case is selected appropriately for the sake of clarity. It is clear from figure 2(a) that for an initial CS with sufficiently small $|\alpha|^2$ (taken to be 1 in this case), Q is roughly oscillatory in time, and takes values ranging from ≈ -0.35 to $\approx +0.05$, during the time interval considered. This behaviour is suggestive of sub-Poissonian statistics over a significant period of time. However, the field also evolves periodically through states displaying Poisson and marginally super-Poisson statistics. Taken together with the behaviour of the SVNE in figure 1(a), it is clear that this oscillatory behaviour reflects the quasiperiodic nature of the dynamics in this case.

In contrast to this, it is evident from figure 2(b) that for the same value of $|\alpha|^2$, an initial field state 10-PACS (which exhibits sub-Poissonian number statistics), evolves through several states which exhibit the same photon number statistics for a significant part of its temporal evolution, with the value of Q always remaining close to its initial value. Interestingly, however, thee are essentially no near-revivals in this case, as is clear from figure 1(b). A similar inference may be drawn from figures 1(c) and 2(c), representing the case in which the initial state of the field is a CS with $|\alpha|^2 = 10$. Its subsequent evolution appears to be through states with marginally sub-Poissonian statistics for a significant part of the time.

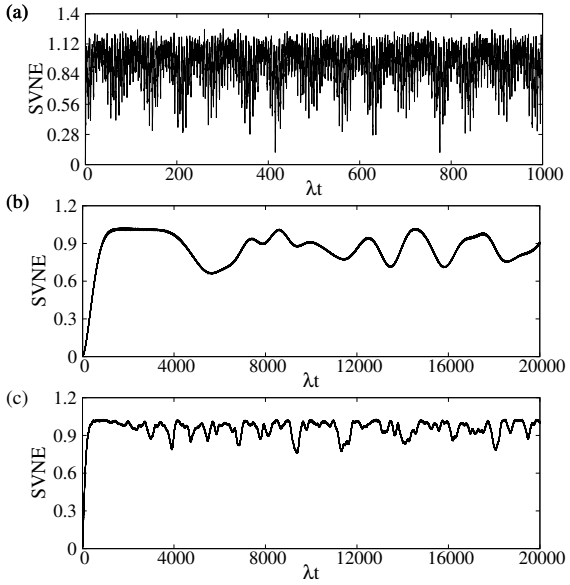

Figure 1: SVNE as a function of the scaled time λt for the three-level V-type atom interacting with a single-mode field, for strong nonlinearity ($\chi/\lambda = 5$). The initial states are (a) $|1;\alpha\rangle$, $|\alpha|^2 = 1$, (b) $|1;\alpha, 10\rangle$, $|\alpha|^2 = 1$, and (c) $|1;\alpha\rangle$, $|\alpha|^2 = 10$.

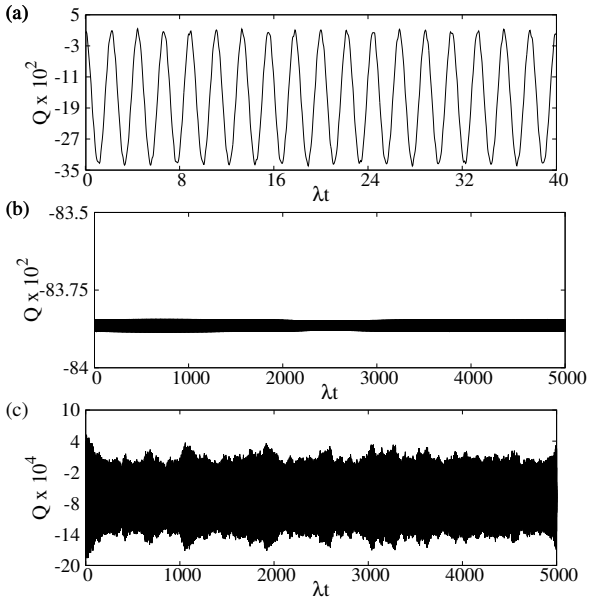

Figure 2: Mandel Q parameter as a function of the scaled time λt for the three-level V-type atom interacting with a single-mode field, for strong nonlinearity ($\chi/\lambda = 5$). The initial states are (a) $|1;\alpha\rangle$, $|\alpha|^2 = 1$, (b) $|1;\alpha, 10\rangle$, $|\alpha|^2 = 1$, and (c) $|1;\alpha\rangle$, $|\alpha|^2 = 10$.

2.2. Interaction with two field modes

We now consider a three-level V-type atom interacting with two field modes, of respective frequencies Ω_1 and Ω_2 and associated operators $(a_1, a_1^\dagger)$ and $(a_2, a_2^\dagger)$. We designate these modes as F_1 and F_2, for convenience. They induce, respectively,

$|3\rangle \leftrightarrow |1\rangle$ and $|3\rangle \leftrightarrow |2\rangle$ transitions. The general Hamiltonian which incorporates nonlinearity in the field modes, intensity-dependent couplings and non-zero detuning parameters is an extension of (2), and is of the form

$$\tilde{H} = \sum_{j=1}^{3} \omega_j \sigma_{jj} + \Omega_1 a_1^\dagger a_1 + \chi_1 a_1^{\dagger 2} a_1^2 + \Omega_2 a_2^\dagger a_2 + \chi_2 a_2^{\dagger 2} a_2^2 + \lambda_1 (R_1 \sigma_{13} + R_1^\dagger \sigma_{31}) + \lambda_2 (R_2 \sigma_{23} + R_2^\dagger \sigma_{32}) \tag{17}$$

where $R_1 = a_1 f_1(N_1)$ and $R_2 = a_2 f_2(N_2)$. As in the bipartite case, we will examine the temporal evolution of the SVNE and the Q parameter corresponding to various initial states of subsystems F_1 and F_2.

Once again, we write $\tilde{H} = \tilde{H}_0 + \tilde{H}_1$, where $[\tilde{H}_0, \tilde{H}_1] = 0$ and

$$\tilde{H}_0 = \omega_3 I + \Omega_1 N_1^{tot} + \Omega_2 N_2^{tot}, \tag{18a}$$

$$\tilde{H}_1 = \chi_1 a_1^{\dagger 2} a_1^2 + \chi_2 a_2^{\dagger 2} a_2^2 - \Delta_1 \sigma_{11} - \Delta_2 \sigma_{22} + \lambda_1 (R_1 \sigma_{13} + R_1^\dagger \sigma_{31}) + \lambda_2 (R_2 \sigma_{23} + R_2^\dagger \sigma_{32}). \tag{18b}$$

As before, $I = \sum_{j=1}^{3} \sigma_{jj}$, $N_1^{tot} = a_1^\dagger a_1 + \sigma_{11}$, $N_2^{tot} = a_2^\dagger a_2 + \sigma_{22}$, and the detuning parameters are

$$\Delta_1 = \omega_3 - \omega_1 + \Omega_1 \tag{19a}$$

$$\Delta_2 = \omega_3 - \omega_2 + \Omega_2. \tag{19b}$$

We have computed the time-dependent density matrix for a generic initial state governed by this Hamiltonian. For the purpose at hand, however, we restrict ourselves to results in the case of zero detuning and intensity-independent couplings. F_1 and F_2 are in initial states given respectively by $\sum_{n=0}^{\infty} q_n |n\rangle$ and $\sum_{m=0}^{\infty} r_m |m\rangle$, and the atom is taken to be in the state $|1\rangle$. In an obvious extension of the notation already used,

$$|\psi(0)\rangle = \sum_{n=0}^{\infty} \sum_{m=0}^{\infty} q_n r_m |1; n; m\rangle . \tag{20}$$

The state of the system at time t in the interaction picture is of the form

$$|\psi(t)\rangle_{int} = \sum_{n=0}^{\infty} \sum_{m=0}^{\infty} q_n r_m \Big\{ A_{nm}(t) |1; n; m\rangle + B_{nm}(t) |2; n+1; m-1\rangle + C_{nm}(t) |3; n+1; m\rangle \Big\}. \tag{21}$$

It is to be understood implicitly that $B_{n0} = 0$.

First, we consider the case $m \geq 1$. It is helpful to define

$$V_{11} = \chi_1 n(n-1), \quad V_{12} = \chi_1 n(n+1) \tag{22a}$$

$$V_{21} = \chi_2 (m-1)(m-2), \quad V_{22} = \chi_2 m(m-1) \tag{22b}$$

$$f_1 = \lambda_1\sqrt{n+1}, \quad f_2 = \lambda_2\sqrt{m}. \tag{22c}$$

Then, the coupled differential equations for the coefficients $A_{nm}(t)$, $B_{nm}(t)$ and $C_{nm}(t)$ are given by

$$i\dot{A}_{nm} = (V_{11} + V_{22})A_{nm} + f_1 C_{nm} \tag{23a}$$

$$i\dot{B}_{nm} = (V_{12} + V_{21})B_{nm} + f_2 C_{nm} \tag{23b}$$

$$i\dot{C}_{nm} = (V_{12} + V_{22})C_{nm} + f_1 A_{nm} + f_2 B_{nm}. \tag{23c}$$

Once again, the trial solution $B_{nm} \sim e^{i\mu t}$ yields the cubic equation (8) for the characteristic frequency μ, but with the coefficients

$$x_1 = V_{11} + 2V_{12} + V_{21} + 2V_{22}, \tag{24a}$$

$$\begin{aligned} x_2 = {} & (V_{12} + V_{21})(V_{11} + V_{12} + 2V_{22}) \\ & + (V_{12} + V_{22})(V_{11} + V_{22}) - f_1^2 - f_2^2, \end{aligned} \tag{24b}$$

$$\begin{aligned} x_3 = {} & (V_{12} + V_{21})\left\{(V_{12} + V_{22})(V_{11} + V_{22}) - f_1^2\right\} \\ & - f_2^2(V_{11} + V_{22}). \end{aligned} \tag{24c}$$

As before, the solutions $\mu_j (j = 1, 2, 3)$ of the cubic equation are of the form written down in (10). The solutions for the coefficients are

$$A_{nm}(t) = \frac{1}{f_1 f_2}\sum_{j=1}^{3} b_j \left\{(\mu_j + V_{12} + V_{22})(\mu_j + V_{12} + V_{21}) - f_2^2\right\} e^{i\mu_j t} \tag{25a}$$

$$B_{nm}(t) = \sum_{j=1}^{3} b_j e^{i\mu_j t} \tag{25b}$$

$$C_{nm}(t) = -\frac{1}{f_2}\sum_{j=1}^{3} b_j(\mu_j + V_{12} + V_{21})e^{i\mu_j t}, \tag{25c}$$

where b_j has the same form as in (13).

Next, consider the case $m = 0$, in which the only possibilities are $|3\rangle \leftrightarrow |1\rangle$ transitions. Equations (23a) and (23c) now reduce to

$$i\dot{A}_{nm} = V_{11}A_{nm} + f_1 C_{nm} \tag{26a}$$

$$i\dot{C}_{nm} = V_{12}C_{nm} + f_1 A_{nm}. \tag{26b}$$

Setting $A \sim e^{i\alpha t}$ yields the secular equation

$$\alpha^2 + y_1\alpha + y_2 = 0 \tag{27}$$

for the characteristic frequency α, where

$$y_1 = V_{11} + V_{12} \tag{28a}$$

$$y_2 = V_{12}V_{11} - f_1^2. \tag{28b}$$

Denoting the solutions of (27) by α_1 and α_2, and using the fact that the initial state of the atom is $|1\rangle$ (so that $A_{nm}(0) = 1, B_{nm}(0) = C_{nm}(0) = 0$), we obtain

$$A_{nm}(t) = \sum_{j=1}^{2} c_j e^{i\alpha_j t} \tag{29a}$$

$$C_{nm}(t) = -\frac{1}{f_1} \sum_{j=1}^{2} c_j(\alpha_j + V_{11}) e^{i\alpha_j t}, \tag{29b}$$

where

$$c_1 = \frac{V_{11} + \alpha_2}{\alpha_2 - \alpha_1} \tag{30a}$$

$$c_2 = \frac{V_{11} + \alpha_1}{\alpha_1 - \alpha_2}. \tag{30b}$$

We now have the complete solution for $|\psi(t)\rangle_{int}$ in explicit form, from which we can construct the density matrix $\rho(t)$ for the system and obtain the reduced density matrix $\rho_{F_1}(t)$ for the field subsystem F_1. The general matrix element of this quantity is given by

$$\begin{aligned} \langle n|\, \rho_{F_1}(t)\, |n'\rangle \;=\; & \sum_{l=0}^{\infty} \Big[q_n q^*_{n'} r_l r^*_l A_{n,l} A^*_{n',l} \\ & + (1-\delta_{n,0})(1-\delta_{n',0}) \\ & \times \{ q_{n-1} q^*_{n'-1} r_{l+1} r^*_{l+1} B_{n-1,l+1} B^*_{n'-1,l+1} \\ & + q_{n-1} q^*_{n'-1} r_l r^*_l C_{n-1,l} C^*_{n'-1,l} \} \Big] \end{aligned} \tag{31}$$

where the t-dependence of A_{nm}, B_{nm}, C_{nm} has been suppressed for simplicity.

Using the reduced density matrix found above, we have investigated in detail the temporal behaviour of the SVNE and the Q parameter. The inferences we draw concerning the dynamics turn out to be consistent with those obtained by treating the atom and the field mode F_2 together as the second subsystem of a bipartite system, and examining its dynamics. As before, we consider (for simplicity) the case $\lambda_1 = \lambda_2 = \lambda$ and $\chi_1 = \chi_2 = \chi$. We set $\chi/\lambda = 5$, in order to facilitate comparison between the present case and the bipartite case considered earlier, as well as the case reported in [13].

Figures 3(a) and (b) depict the SVNE for the subsystem F_1 as a function of the scaled time λt, for initially unentangled states $|1; \alpha; \alpha\rangle$ with $|\alpha|^2 = 1$ and $|\alpha|^2 = 10$ respectively. It is evident (see figure 3(a)) that the tripartite case is bereft of even near-revivals, in the regime of strong nonlinearity, even for small values of $|\alpha|^2$. This is in contrast to figure 1(a) (which also corresponds to $|\alpha|^2 = 1$), and is akin to the situation reported in [13], where each of the two subsystems of the bipartite system had 'large' Hilbert spaces, in contrast to the bipartite system considered earlier in this paper. This indicates that even if two subsystems of a full system are significantly 'large' (in the sense of a high-dimensional Hilbert space), the revival phenomenon is absent for sufficiently

strong nonlinearities, independent of whether these large subsystems interact with each other directly or through much smaller subsystems.

For the same tripartite initial states as in figures 3(a) and (b), we have plotted the Q parameter as a function of λt in figures 4(a) and (b). Once again we note that an initial coherent state of the subsystem evolves through a series of mixed states with sub-Poissonian number statistics for a significant part of the time, and through other mixed states also having Poissonian number statistics. The somewhat oscillatory nature of Q for small $|\alpha|^2$ as in figure 4(a) is replaced by bursts of oscillations in figure 4(b). The absence of revivals of the initial state $|1;\alpha;\alpha\rangle$ with $|\alpha|^2 = 10$, taken together with the absence of regular oscillatory behaviour of Q for this state as it evolves in time, suggests that a detailed time series analysis of an appropriate observable such as the mean photon number would reveal a rich diversity of ergodicity properties. For ready comparison, a similar analysis is necessary for appropriate initial states of the bipartite model of the previous subsection. These results are presented in the next section.

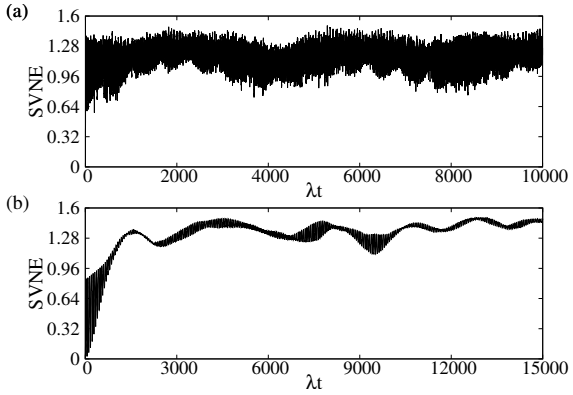

Figure 3: SVNE as a function of scaled time λt for the three-level V-type atom interacting with two fields modes, for strong nonlinearity ($\chi/\lambda = 5$) and initial states (a) $|1;\alpha;\alpha\rangle$, $|\alpha|^2 = 1$, and (b) $|1;\alpha;\alpha\rangle$, $|\alpha|^2 = 10$.

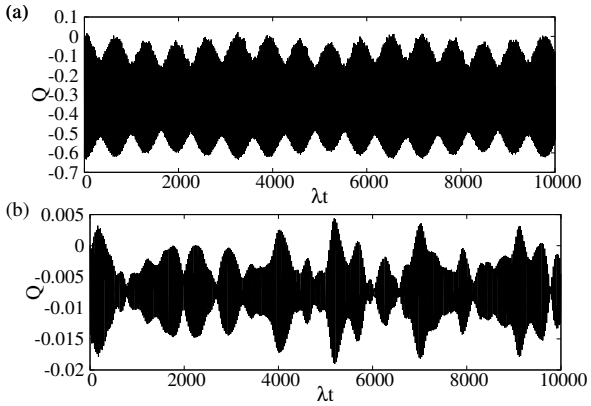

Figure 4: Mandel Q parameter as a function of scaled time λt for the three-level V-type atom interacting with two fields modes, for strong nonlinearity ($\chi/\lambda = 5$) and initial states (a) $|1;\alpha;\alpha\rangle$, $|\alpha|^2 = 1$, and (b) $|1;\alpha;\alpha\rangle$, $|\alpha|^2 = 10$.

3. Ergodicity properties of the mean photon number

We are now in a position to investigate the dynamics of any appropriate observable in both the models described in Section 2. In order to be specific, we examine in detail the ergodicity properties of the mean photon number $\langle a^\dagger a\rangle$ of the radiation field as it interacts with the three-level atom in the bipartite model, and the mean photon number $\langle a_1^\dagger a_1\rangle$ of F_1 in the tripartite model. The procedure we adopt is as follows. Starting with a specified initial state of the full system, we generate a sufficiently long time series of the mean photon number (approximately 10^7 data points obtained in time steps δt). The time in units of δt is denoted by τ. The interval of values of the mean photon number is coarse-grained into small equal-sized cells, and the distribution of the time of the first recurrence to a given generic cell is determined. The plot of the observable at time $\tau+1$ versus its value at time τ (the return map) has been obtained for different initial states. Further, we have carried out a detailed time series analysis including estimation of the minimum embedding dimension, phase space reconstruction, and determination of the maximum Lyapunov exponent.

Before presenting our results, we summarize briefly the inferences drawn in [21] based on a similar study undertaken on the bipartite model of [12]. There, too, the observable whose time series was analyzed was the mean photon number. The first return distributions for various initial coherent states with small $|\alpha|^2$, were spiky, and the corresponding Lyapunov exponents were zero, signalling regular quasiperiodic behaviour [19] of the observable concerned. In contrast, in all cases where the initial state was a CS with large $|\alpha|^2$ or a PACS, the first return dustribution was exponential and the Lyapunov exponent was positive, thereby indicating exponentially unstable dynamics. Both subsystems in this model had infinite-dimensional Hilbert spaces, in contrast to the two models considered in the present work, where the atomic transitions are confined to just three levels and the two radiation fields in the tripartite model do not directly interact with each other. There is therefore no reason to expect, à priori, that the inferences drawn in [21] will hold good here.

We start with the bipartite system of the three-level atom interacting with a single field mode. The first task is to verify if the dynamics is metrically transitive for generic cells in the coarse-grained phase space of the mean photon number. Figure 5 is a plot of the mean recurrence time versus cell size for an initial state $|1;\alpha\rangle$ with $|\alpha|^2 = 10$. We have used 10^7 data points with a time step 0.005. The excellent linear fit confirms that the Poincaré recurrence theorem is satisfied, confirming that the dynamics is ergodic.

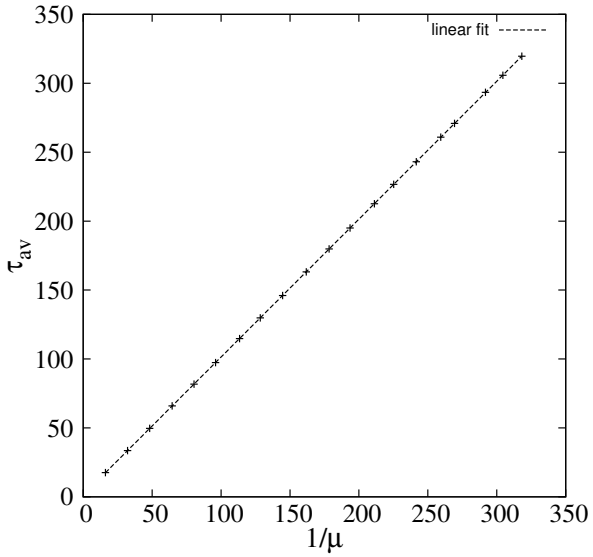

Figure 5: Mean recurrence time of the mean photon number to a cell versus the reciprocal of its invariant measure, for the bipartite system. Initial state $|1;\alpha\rangle$, with $|\alpha|^2 = 1$.

Figure 6(a) shows the spiky first-return-time distribution ϕ_1 to a generic cell for an initial state $|1;\alpha\rangle$ for $|\alpha|^2 = 1$. Its spiky nature is an indication that the dynamics is quasiperiodic with several incommensurate frequencies [19]. With an increase in $|\alpha|^2$ to the value 10, the distribution becomes exponential, as seen in figure 6(b). The latter is the distribution expected for a hyperbolic dynamical system for a sufficiently small cell size [24, 25]. We have further confirmed in this case, from the distributions for two, three and four successive recurrences to a generic cell, that such returns are uncorrelated, being given by the successive terms of a Poisson distribution [26, 27].

We have also carried out a detailed time-series analysis of the mean photon number for the initial states $|1;\alpha\rangle$ with $|\alpha|^2 = 1$ and $|1;\alpha,1\rangle$ with $|\alpha|^2 = 10$, with respective time steps of 0.25 and 0.005. This study comprises phase space reconstruction, estimation of the minimum embedding dimension by the false-nearest-neighbours (FNN) algorithm [28, 29], and calculation of the maximal Lyapunov exponent using a robust algorithm by Rosenstein et al. [30]. The algorithms have been implemented with the package TISEAN [31]. In both cases ($|\alpha|^2 = 1$ and $|\alpha|^2 = 10, m = 1$) the Lyapunov exponent is found to be zero. While this is consistent with the conclusion arrived at in [21] for a spiky first return distribution (Figure 6(a)), it is rather surprising in the case of an exponential first return distribution (which obtains for the initial state $|1;\alpha,1\rangle$ with $|\alpha|^2 = 10$), as the latter is customarily associated with hyperbolicity. Evidently, the limited nature of the transitions allowed for the atomic subsystem in this case plays a crucial role in determining the ergodicity properties of the observable.

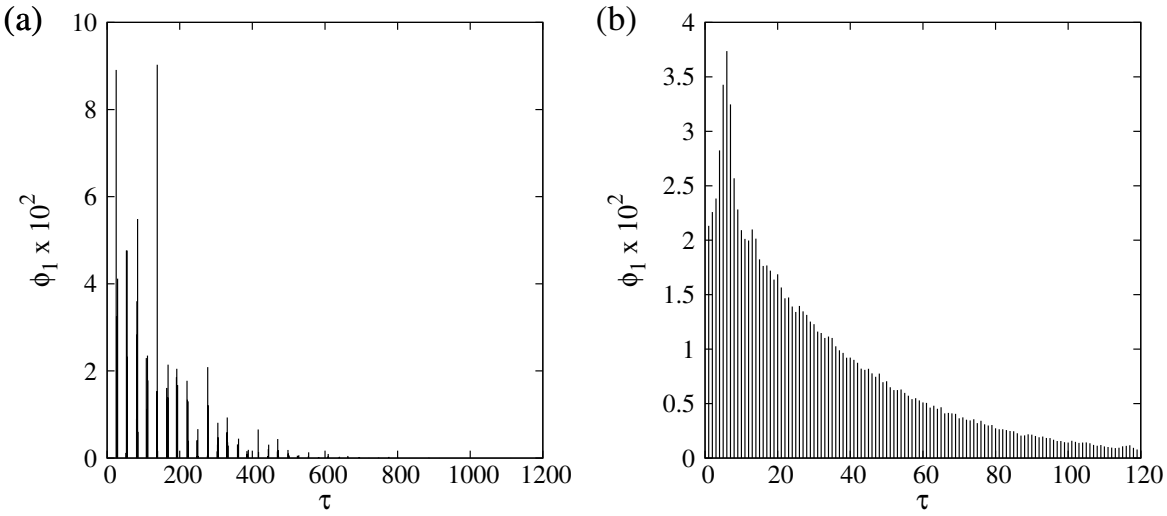

Figure 6: First-return-time distribution ϕ_1 of the mean photon number $\langle a^\dagger a\rangle$ for the bipartite system. Initial state (a) $|1;\alpha\rangle$, $|\alpha|^2 = 1$, and (b) $|1;\alpha\rangle$, $|\alpha|^2 = 10$

Figures 7(a)-(c) depict the return maps of the mean photon number in the bipartite model for initial states $|1;\alpha\rangle$ with $|\alpha|^2 = 1$, $|1;\alpha, 10\rangle$, $|\alpha|^2 = 1$, and $|1;\alpha\rangle$ with $|\alpha|^2 = 10$ respectively. We have used 3×10^5 data points for generating these maps, with a time step 0.25 in figure 7(a) and 0.005 in figures 7(b) and (c). As expected, for an initial CS with a small value of $|\alpha|^2$ (figure 7(a)), the return map is an annulus with no sub-structure. For an initial PACS with the same small value of $|\alpha|^2$, the annulus is considerably broadened, and has sub-structures in it (figure 7(b)). These features are consistent with corresponding first-return distributions that are spiky and vanishing Lyapunov exponents. In contrast, the return map (figure 7(c)) for an initial CS with large $|\alpha|^2$ is seen to tend towards the space-filling map reminiscent of a ' chaotic' system, although the Lyapunov exponent remains zero in this case. We therefore conclude that, in the presence of a subsystem with a low-dimensional Hilbert space, exponential first return time distributions and space-filling return maps merely signal hyperbolicity without necessarily implying chaotic behaviour (as characterized by a positive Lyapunov exponent).

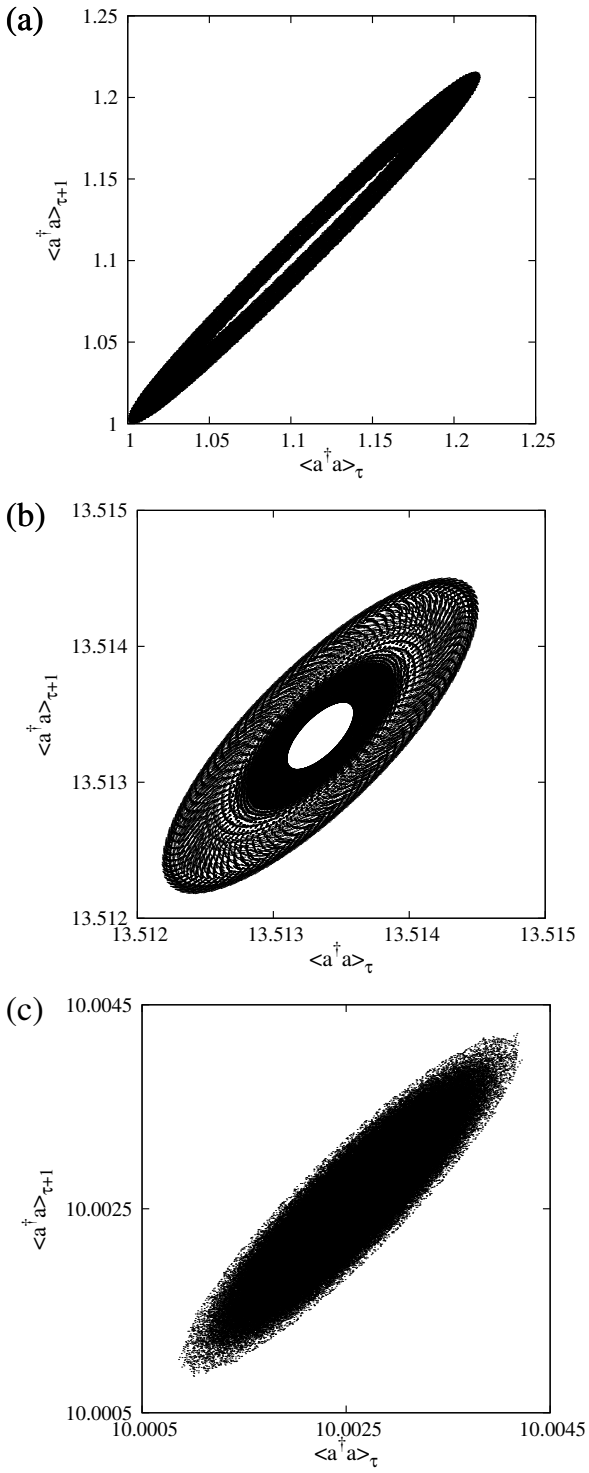

Figure 7: Return maps of the mean photon number $\langle a^\dagger a\rangle$ in the bipartite system. Initial states (a) $|1;\alpha\rangle$ $|\alpha|^2 = 1$, (b) $|1;\alpha,10\rangle$ $|\alpha|^2 = 1$, and (c) $|1;\alpha\rangle$ $|\alpha|^2 = 10$

Turning to the tripartite (or two field modes plus atom) model, we have studied extensively the recurrence statistics of the mean photon number of one of the field modes, for various initial states, and for different ratios of the strength of the nonlinearities to the

corresponding interaction strengths. In order to compare our results with the bipartite model considered above, and with the results of [21], we present relevant plots in the illustrative case of the initial state $|1;\alpha;\alpha\rangle$ with $|\alpha|^2 = 10$, setting $\chi_1/\lambda_1 = \chi_2/\lambda_2 = 5$. A long time series ($3\times10^5$ data points with time step equal to unity) of the mean photon number $\langle a_1{}^\dagger a_1\rangle$ was generated for implementimg the FNN algorithm and computing the Lyapunov exponent.

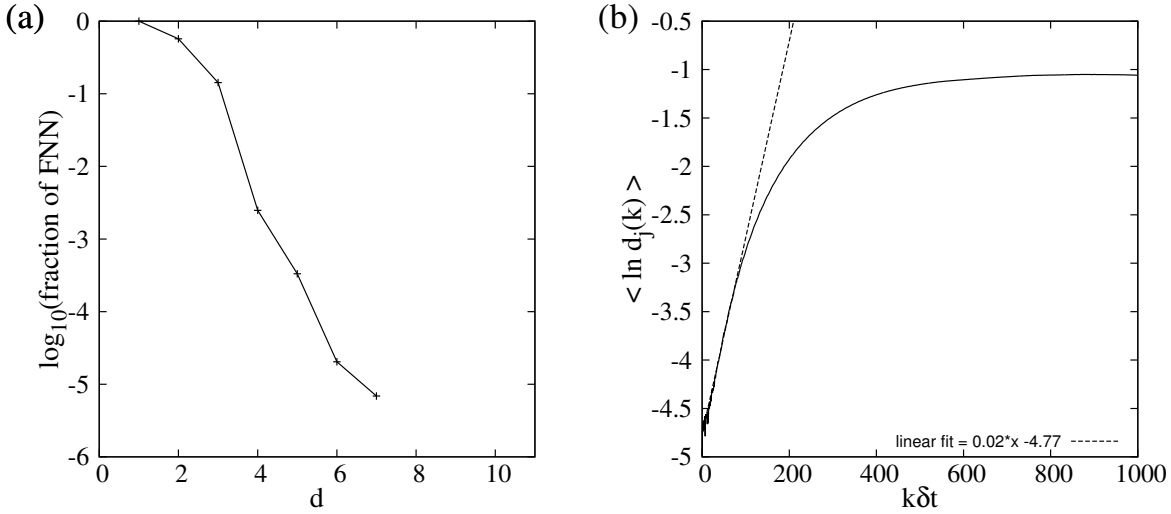

Figure 8: (a) Fraction of FNN versus embedding dimension d, and (b) $\langle \ln d_j(k)\rangle$ versus $t(= k\delta t)$ using the algorithm of Rosenstein et al., for the initial state $|1;\alpha;\alpha\rangle$, $|\alpha|^2 = 10$ for the tripartite system. The maximal Lyapunov exponent is ≈ 0.02.

Figure 8(a) shows the fraction of FNN as a function of the embedding dimension d. We estimate the minimum embedding dimension to be 7, as the fraction of FNN becomes negligible ($< 10^{-5}$) beyond this value. Using this, we have assessed the extent of the sensitivity to initial conditions displayed in the reconstructed phase space by computing the Lyapunov exponent from the time series of $\langle a_1{}^\dagger a_1\rangle$. The initial set of separations $\{d_j(0)\}$ between the jth pair of nearest neighbours evolves to $\{d_j(k)\}$ after k time steps. As is well known, the maximal Lyapunov exponent is the slope of the linear region that lies between the initial transient and the final saturation region in the plot of $\langle \ln\, d_j(k)\rangle$ versus time (figure 8(b)). Here, the average is over all values of j. The maximal Lyapunov exponent is estimated to be ≈ 0.02, indicative of weakly chaotic behaviour. On the other hand, the corresponding first-return-time distribution to a generic initial cell (figure 9) obtained from a sample set of 10^7 data points for the same initial state and parameter values is spiky, contrary to what we would expect. We note, however, that the spiky distribution shows signs of tending to an exponential one, as can be seen from the envelope of the spikes. Once again, the low dimensionality of the atomic Hilbert space appears to be responsible for these features.

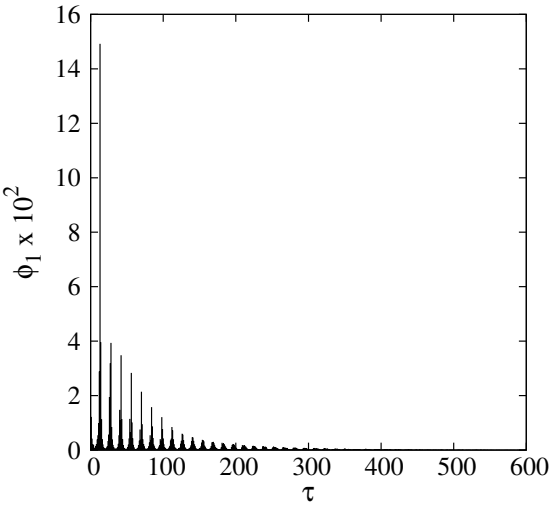

Figure 9: First-return-time distribution ϕ_1 of the mean photon number $\langle {a_1}^\dagger a_1 \rangle$ in the tripartite model. Initial state $|1;\alpha;\alpha\rangle$ with $|\alpha|^2 = 10$

4. Concluding remarks

Our investigations reveal interesting and somewhat counter-intuitive results on the dynamics of interacting atom-field systems. Independent of whether the radiation fields in a multipartite system exhibit ideal coherence or significant departures from coherence, the number statistics and the extent of entanglement of the various subsystems with each other during temporal evolution are affected significantly by the 'smallness' of the atomic Hilbert space.

The recurrence time distribution ϕ_1 of an observable to cells in a coarse-grained phase space of relevant observables of a system is an important quantifier of the nature of the dynamics. A spiky ϕ_1 is generally indicative of quasiperiodicity, while an exponential distribution is a generic characteristic of hyperbolicity in the dynamics. The latter need not imply, however, the positivity of any of the Lyapunov esponents. Similarly, a spiky form of ϕ_1 could accompany weakly chaotic behaviour as indicated by a small positive Lyapunov exponent. Both these uncommon features are exhibited by the models we have studied in this paper.

The strength of the nonlinearity in the field modes is the underlying feature that leads to a wide range of ergodicity properties of the mean photon number. In the presence of a sufficiently strong atom-field coupling, the field mode evolves through a spectrum of states with different number statistics. It may be possible to reconstruct the latter through continuous variable quantum state tomography. An appropriate weak local probe can be used to determine the mean photon number of the field, and homodyne correlation measurements on the lines suggested in [14, 32] can perhaps be used to measure relevant observables.

References

[1] Robinett R W 2004 *Phys. Rep.* **392** 1
[2] Milburn G J 1986 *Phys. Rev.* A **33** 674
[3] Kitagawa M and Yamamoto Y 1986 *Phys. Rev.* A **34** 3974
[4] Averbukh I Sh and Perelman N F 1989 *Phys. Lett.* A **139** 449
[5] Greiner M, Mandel O, Hänsch T W and Bloch I 2002 *Nature* **419** 51
[6] Tara K, Agarwal G S and Chaturvedi S 1993 *Phys. Rev.* A 47 5024
[7] Miranowicz A, Tanaś R and Kielich S 1990 *Quantum Opt.* **2** 253
[8] Yurke B and Stoler D 1986 *Phys. Rev. Lett.* **57** 13
[9] Sudheesh C, Lakshmibala S and Balakrishnan V 2004 *Phys. Lett.* A **329** 14
[10] Sudheesh C, Lakshmibala S and Balakrishnan V 2005 *Europhys. Lett.* **71** 744
[11] Zavatta A, Viciani S and Bellini M 2004 *Science* **306** 660
[12] Agarwal G S and Puri R R 1989 *Phys. Rev.* A **39** 2969
[13] Sudheesh C, Lakshmibala S and Balakrishnan V 2006 *J. Phys.* B **39** 3345
[14] Webb J G, Ralph T C and Huntington E H 2006 *Phys. Rev.* A **73** 033808
[15] Sudheesh C, Lakshmibala S and Balakrishnan V 2009 *Phys. Lett.* A **373** 2814
[16] Kac M 1947 *Bull. Am. Math. Soc.* **53** 1002
[17] Chirikov B V and Shepelyansky D L 1999 *Phys. Rev. Lett.* **82** 528; Zaslavsky G M and Edelman M 2001 *Chaos* **11** 295; Artuso R, Cavallasca L and Cristadoro G 2008 *Phys. Rev.* E **77** 046206; Altmann E G and Tel T 2008 *Phys. Rev. Lett.* **100** 174101
[18] Balakrishnan V, Nicolis G and Nicolis C 1997 *J. Stat. Phys.* **86** 191
[19] Nicolis C, Nicolis G, Balakrishnan V and Theunissen M 1997 *Stochastic Dynamics* (Lecture Notes in Physics Vol. 484) ed Schimansky-Geier L and Poschel T (Berlin/Heidelberg: Springer-Verlag)
[20] Eckmann J-P, Kamphorst S O and Ruelle D 1987 *Europhys. Lett.* **4** 973; Marwan N, Wessel N, Meyerfeldt U, Schirdewan A and Kurths J 2002 *Phys. Rev.* E **66** 026702; Marwan N, Romana M C, Thiel M and Kurths J 2007 *Phys. Rep.* **438** 237
[21] Sudheesh C, Lakshmibala S and Balakrishnan V 2010 *EPL* **90** 50001
[22] McKeever J, Boca A, Boozer A D, Buck J R and Kimble H J 2003 *Nature* **425** 268
[23] R.A. Zait 2003 *Phys. Lett.* A **319** 461
[24] Hirata M 1993 *Ergod. Th. Dyn. Systems* **13** 533
[25] Balakrishnan V and Theunissen M 2001 *Stoch. Dyn.* **1** 339
[26] Hirata M 1995 *Dyn. Syst. Chaos* **1** 87
[27] Balakrishnan V, Nicolis C and Nicolis G 2001 *Stoch. Dyn.* **1** 345
[28] Kennel M B, Brown R and Abarbanel H D I 1992 *Phys. Rev.* A **45** 3403
[29] Abarbanel H D I 1996 *Analysis of Observed Chaotic Data* (Berlin/New York: Springer-Verlag)
[30] Rosenstein M T, Collins J J and de Luca C J 1993 *Physica* D **65** 117
[31] Hegger R, Kantz H and Schreiber T 1999 *Chaos* **9** 413
[32] Shchukin E V and Vogel W 2005 *Phys. Rev.* A **72** 043808